Size-scale and slenderness influence on the compressive strain-softening behaviour of concrete

A. CARPINTERI[1], F. CIOLA[1], N. PUGNO[1], G. FERRARA[2] and M. E. GOBBI[2]

[1]*Department of Structural Engineering and Geotechnics, Politecnico di Torino, Corso Duca degli Abruzzi 24, 10129 Torino, Italy*
[2]*ENEL-CRIS, Milano, Italy*

Received in final form 9 February 2001

ABSTRACT In this article the compressive mechanical behaviour of quasi-brittle materials is analysed by means of experimental tests and by using an *ad hoc* algorithm for numerical simulations based on the Pseudo-traction and the Boundary-element methods. The experimental analysis is carried out on specimens with three different size-scales, three different values of slenderness and two boundary conditions. The numerical analysis was carried out by taking into account the initial random crack distribution, considering the mutual crack interaction, the crack–boundary interaction and the internal friction between the faces of the cracks. The numerical results, in good agreement with the experimental data, highlight the characteristic strain-softening behaviour of quasi-brittle materials, and the influence of size-scale and slenderness on the structural response. By observing the evolution of the crack patterns, it is possible to emphasize, both experimentally and numerically, the transition from crushing to splitting collapse by increasing the specimen slenderness, as well as the transition from ductile to brittle behaviour by increasing the specimen size-scale.

Keywords boundary-elements; compression; multi-cracked finite plate; pseudo-traction method; quasi-brittle materials.

NOMENCLATURE

a, b = auxiliary constants
C = global compliance
C' = elastic compliance
C'' = cracks-compliance
E = elastic modulus
E^* = fictitious elastic modulus
F = compressive normal force
λ = internal friction coefficient
K_{eq} = equivalent stress-intensity factor
K_I = stress-intensity factor for mode I
K_{IC} = critical stress-intensity factor
K_{II} = stress-intensity factor for mode II
W = strain energy density
σ = compressive normal stress
$\mathcal{G}_I$ = fracture surface energy
τ = shearing stress
τ_{eff} = effective shearing stress
τ_f = friction shearing stress
θ = crack propagation angle

Correspondence: A. Carpinteri, Department of Structural Engineering and Geotechnics, Politecnico di Torino, Corso Duca degli Abruzzi 24, 10129 Torino, Italy.
E-mail: carpinteri@polito.it.

INTRODUCTION

The study of the compressive mechanical behaviour of concrete, which has already been analysed by several authors, still does not present a complete and systematic treatment, even if many salient aspects have already been emphasized. The most important of these aspects is the phenomenon of strain-softening that presents variable characteristics by varying the test conditions. There are in fact many parameters to be taken into account, and the two most important are the slenderness of the specimen and the friction between the specimen and the loading platens.

The present investigation highlights these aspects experimentally and numerically. The experimental analysis was carried out at the ENEL-CRIS Laboratories in Milan,[1] within the framework of the Round-Robin Test promoted by RILEM TC 148-SSC, whereas an *ad hoc* algorithm based on the Pseudo-traction and on the Boundary-element methods was implemented and utilized for numerical simulations.

EXPERIMENTAL INVESTIGATION

The experimental tests have been carried out on concrete specimens characterized by the following parameters:

- one quality of concrete (normal strength concrete);
- three specimen sizes: prisms with square bases of side length 50, 100 and 150 mm;
- three values of slenderness (height/square base side equal to 0.5, 1 and 2);
- two boundary conditions (with and without friction).

With regard to concrete quality, only one type of concrete was used with the following composition:

- 425 Portland cement with a batching of 375 kg m^{-3};
- water to cement ratio equal to 0.5;
- aggregates with the size distribution shown in Table 1.

The casting procedure was the following. The concrete was poured in the moulds, and compacted on a vibration table for 30 s. The specimens were then kept in the moulds for 2 days, at 90% relative humidity under wet cloths. After demoulding, the specimens were placed in a fresh water basin at 20 °C. Sawing of the specimens was carried out at the age of 14 days.

It is important to emphasize that the specimens were not obtained directly; larger blocks were previously cast, from which the prisms were afterwards sawn. In this regard, details are shown in Table 2.

Table 2 Block-specimen basis dimensions

Block dimensions (mm^3)	Specimen base dimensions (mm^2)
100 × 100 × 500	prisms 50 × 50
150 × 150 × 600	prisms 100 × 100
200 × 200 × 600	prisms 150 × 150

The direction of loading in the compression test was perpendicular to the direction of casting, to remove the weak top layer that could lead to flexural stresses. All the specimens were cut by diamond grinding discs. Their bases, which were in contact with the loading platens, were ground flat by the flattening machine. After sawing, the specimens were kept in the water basin for 28 days. At this age they were sealed in plastic bags and kept in a 90% relative humidity chamber until the moment of testing. In order to guarantee perfect contact between the loading platens and the specimens, a cement capping was performed before beginning the tests, at an age of 11 weeks.

One of the purposes of the present research is to determine the effect of frictional restraint between specimen and loading platens on the experimental response.

The two testing machines (of different stiffness and loading capacity) were equipped with rigid steel platens, i.e. without rotation capability. The rigid loading platens present the same square cross-section for prisms. The direct contact of the specimen with the loading platens produces friction conditions at the interface, because the concrete lateral expansion is suppressed. Among the various frictionless loading systems, the application of teflon interlayers (friction coefficient ≈ 0.01, thickness of 5 mm, ungreased) between specimen and steel platens was chosen.

The measurement of the load, performed by a dynamometric cell, was directly transmitted to the data acquisition system. The overall vertical displacement was measured with inductive displacement transducers with ±5 mm of stroke and a sensitivity of 1.25 μm. The average value from the vertical transducers served as feed-back signal in the closed-loop servo-control. The loading rate was 1 μm s^{-1}.

The arrangement of the vertical transducers allows measurements including the deformation of the steel platens, of the teflon interlayers and strain of cement capping, in addition to the specimen deformation. To obtain the correct strain value, it was necessary to

Table 1 Size distribution of aggregates

Size (mm)	0.125–0.25	0.25–0.5	0.5–1.0	1.0–2.0	2.0–4.0	4.0–8.0
Distribution (kg m^{-3})	127	234	272	272	363	540

eliminate from the measurement these unwanted contributions. This was achieved by evaluating such a contribution using some load tests carried out only on steel plates and on steel plates coupled to a teflon layer or coupled to a mortar layer. After this we evaluated the strain contribution of the capping directly on a concrete specimen as the difference between the total strain (plates + concrete + capping + teflon) and the concrete strain, measured by vertical transducers directly glued to the lateral surface of the specimen, near its base.[1]

NUMERICAL ANALYSIS

To interpret the experimental data, a set of two-dimensional numerical simulations was carried out, by developing an *ad hoc* algorithm.

The numerical algorithm is based on the Pseudo-traction and on the Boundary-element methods and allows one to represent the stress field in a finite plate with several cracks as the superposition of elementary cases.

The Pseudo-traction method was developed by Horii and Nemat-Nasser,[2] Kachanov and Montagut[3] and Kachanov[4] and it is based on the superposition principle (Fig. 1). Scheme (a) in Fig. 1 is treated by the Boundary-element method;[5,6] on the other hand, the analysis of the stress field in schemes (b) and (c) of Fig. 1 is performed by referring to Sneddon's formulation.[7] This was also assumed by Yang and Liu,[8] Carpinteri *et al.*[9] and Carpinteri and Yang,[10–12] and provides the stress field as a function of normal and shearing stresses acting directly on the crack edges.

Using the Sneddon formulation and applying the Pseudo-traction and the Boundary-element methods, a linear system may be written, the solution of which provides the normal and shearing stresses acting on the crack edges in schemes (b) and (c). The determination of the stress-intensity factors K_I and K_{II} is made by considering the mutual crack interaction as well as the crack–boundary interaction.[13–15] In addition, it is possible to take into account the internal friction between the faces of the crack. When compressive normal stresses act on the crack surfaces, friction shearing stresses $\tau_f = \lambda\sigma$ appear, suppressing relative slippage (λ is the internal friction coefficient).

If shearing stresses are active on the crack, the effect of these is diminished by the friction shearing stresses. If $|\tau| > |\lambda\sigma|$ the effective stress is:

$$\tau_{\text{eff}} = \tau\left(1 - \frac{|\lambda\sigma|}{|\tau|}\right) \tag{1}$$

If $|\tau| < |\lambda\sigma|$, we impose $\tau_{\text{eff}} = 0$. By using the concept of effective stress τ_{eff}, it is possible to compute the stress-intensity factors taking into account the internal friction. The above formulation may be easily extrapolated to multicracked geometries.

In order to study the experiments in a realistic way, it is impossible to leave out of consideration the random distribution of cracks initially present in the material. The internal damage develops over three different scale levels (micro-, meso- and macrocracks) and is present even before the loading process.

In connection with what has been written above, a structural scheme constituted by a finite plate with a random distribution of initial meso- and macrocracks was adopted in the numerical simulations. Starting from this geometry and using the above mentioned formulation, the stress field and the stress-intensity factors acting on each crack were calculated. Then, referring to the well-known maximum hoop stress criterion,[16] for each crack tip a propagation angle θ and an equivalent stress-intensity factor K_{eq} can be defined as:

$$K_I \sin(\theta) + K_{II}(3\cos(\theta) - 1) = 0 \tag{2}$$

$$K_{eq} = \cos\left(\frac{\theta}{2}\right)\left(K_I \cos^2\left(\frac{\theta}{2}\right) - \frac{3}{2} K_{II} \sin(\theta)\right) \tag{3}$$

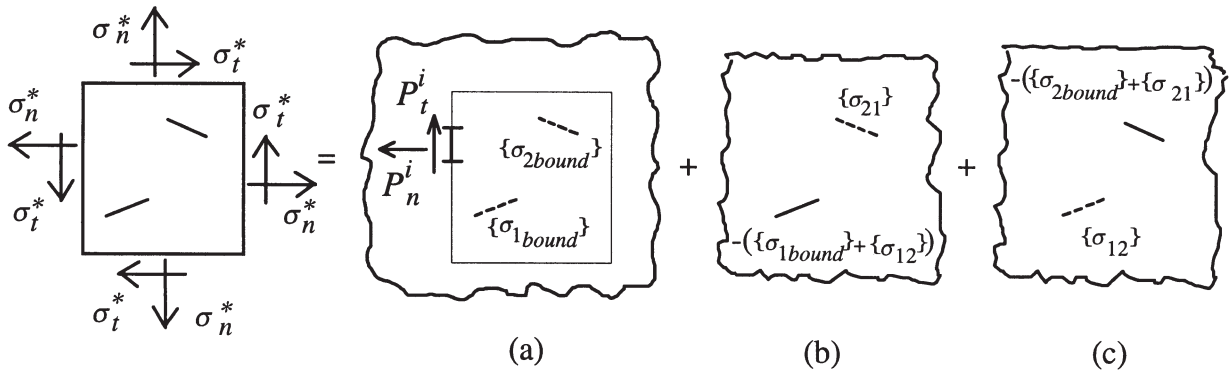

Fig. 1 Schemes for the application of the superposition principle.

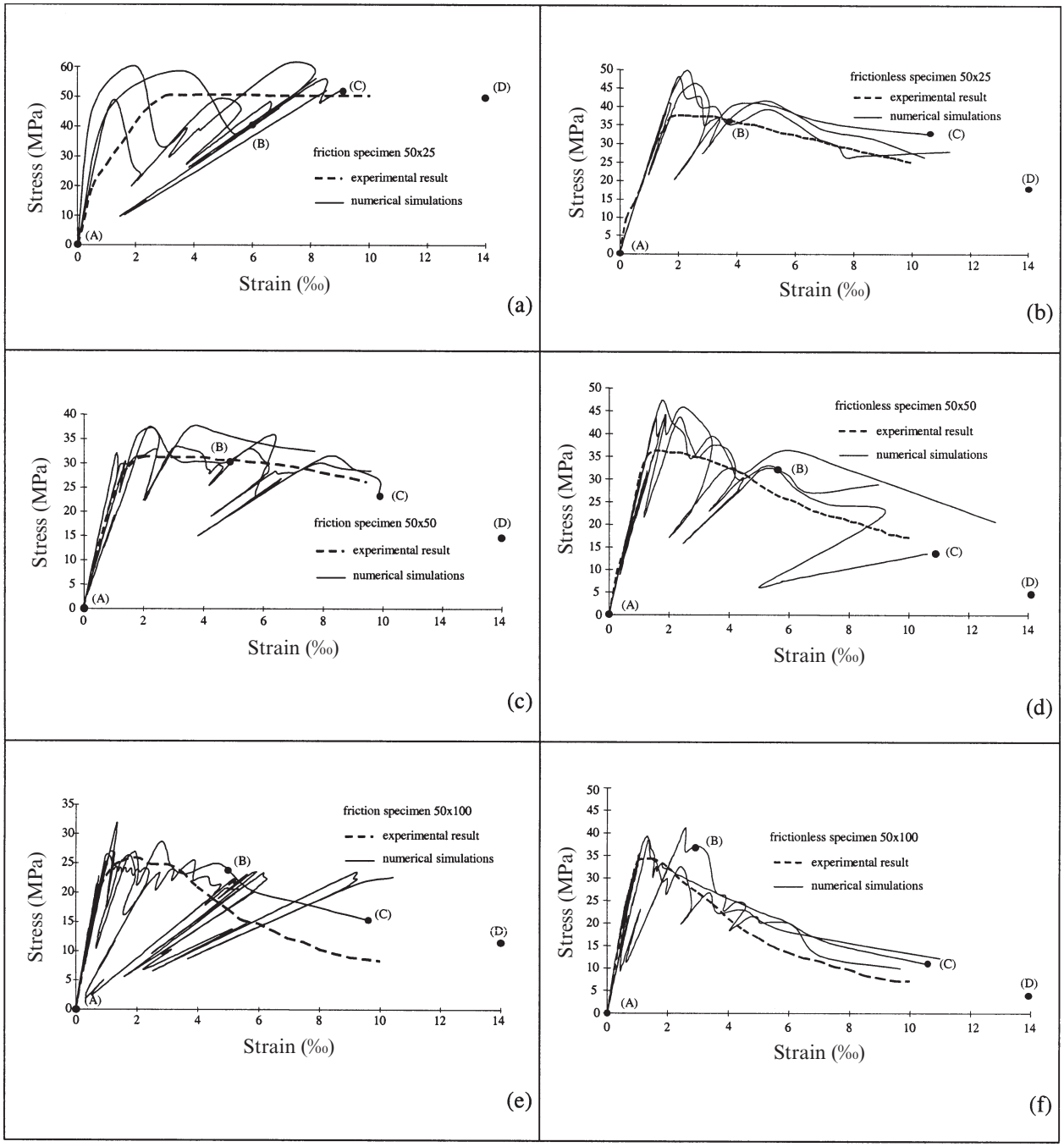

Fig. 2 Stress–strain diagrams (base sides = 50 mm × 50 mm).

where K_I and K_{II} are the stress-intensity factors for the mode I and II, respectively, so that the crack with the highest K_{eq} can be selected. Comparing the highest K_{eq} with the critical value K_{IC}, the external load of crack propagation can be calculated.

The next step is to cause the crack to propagate by a finite amount at the tip. At this stage, we are faced with a new geometry, on which it is necessary to carry out a fresh analysis. The procedure is then iterated until the specimen completely collapses. In this way, it is possible to follow the crack pattern evolution during the loading process, computing the critical load at each step.

With regard to the deformation response of the specimen, it is necessary to define a fundamental parameter represented by the global compliance. This is provided by two contributions: the former, C', is spread and

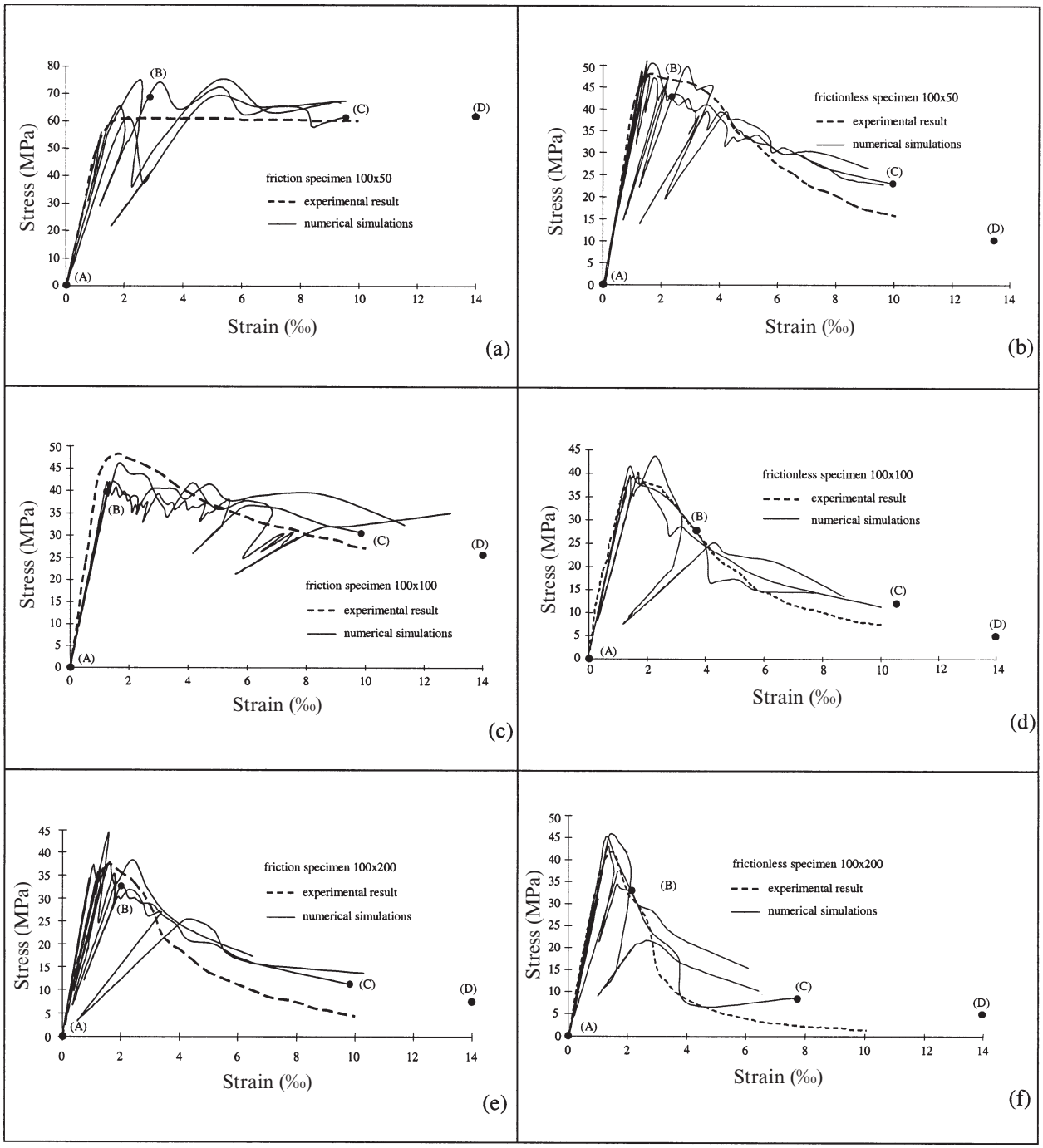

Fig. 3 Stress–strain diagrams (base sides = 100 mm × 100 mm).

depends on the specimen dimensions and on the elastic modulus (compliance of the uncracked linear elastic plate); the latter is due to the meso- and macro-cracks and is called incremental compliance, C''. Both the compliances, C' and C'', vary during the loading simulation.

If a propagating crack is considered, using Clapeyron's Theorem (see Carpinteri[17]) and the principle of conservation of energy, the following balance can be written:

$$\mathcal{G}_{\mathrm{I}} = \frac{1}{2} F^2 \frac{\partial C}{\partial A} = \frac{K_{\mathrm{I}}^2}{E} + \frac{K_{\mathrm{II}}^2}{E} \tag{4}$$

where $\mathcal{G}_{\mathrm{I}}$ is the fracture energy per unit area, F is the

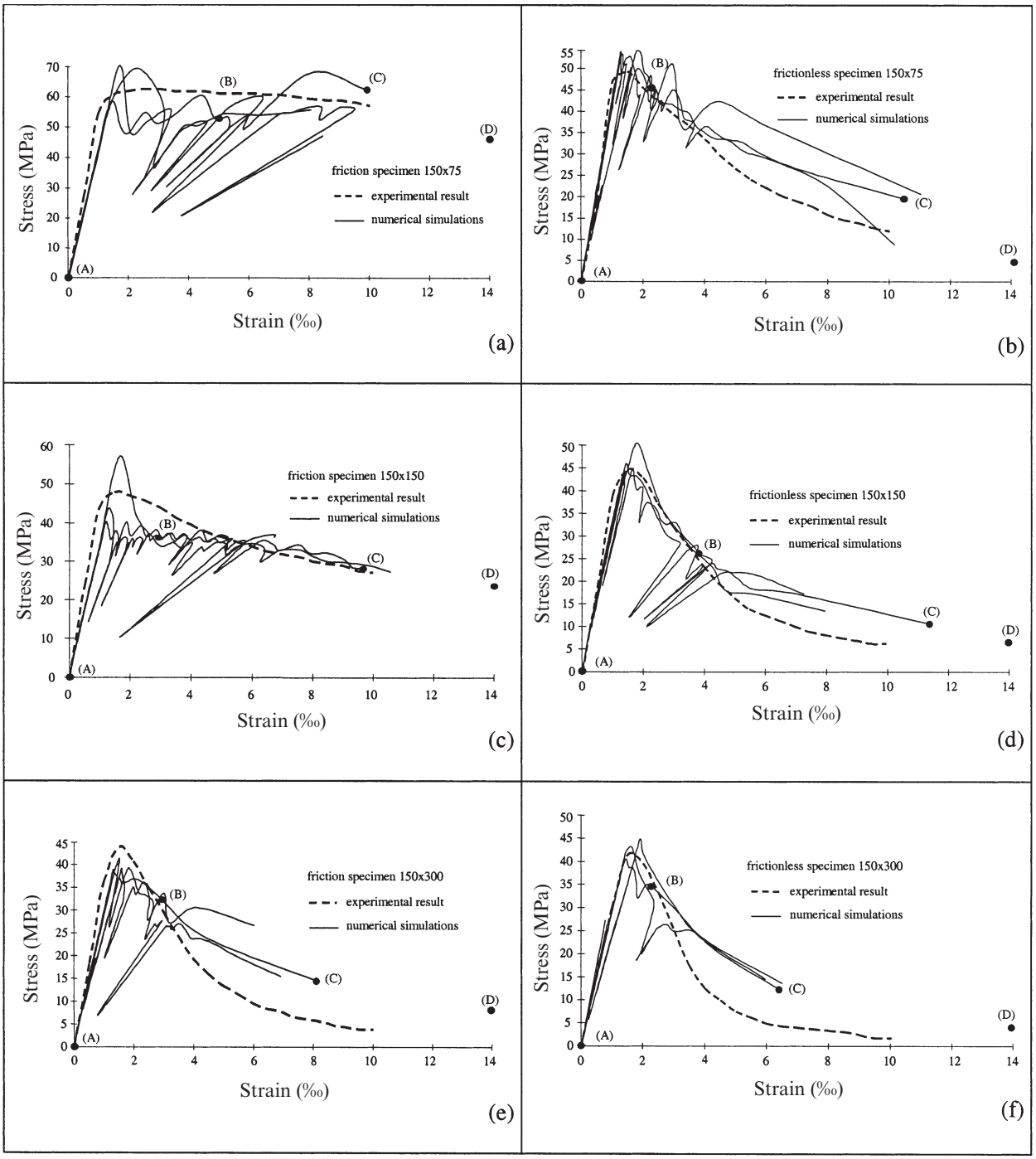

Fig. 4 Stress–strain diagrams (base sides = 150 mm × 150 mm).

applied load, C is the compliance of the cracked plate and A is the crack area. It is important to observe that $\partial C/\partial$A is evidently equal to $\partial C''/\partial A$. The variation of C'' during the propagation of the crack can be calculated from Eq. (4).

With regard to the compliance contribution C' due to the material elasticity, the constancy assumption for the material elastic modulus does not reflect the physical evolution of the phenomenon. In fact, during the loading process, the microcracks, approximately distributed in a uniform manner, grow in the material, so that their macroscopic effect is the progressive decay of bulk

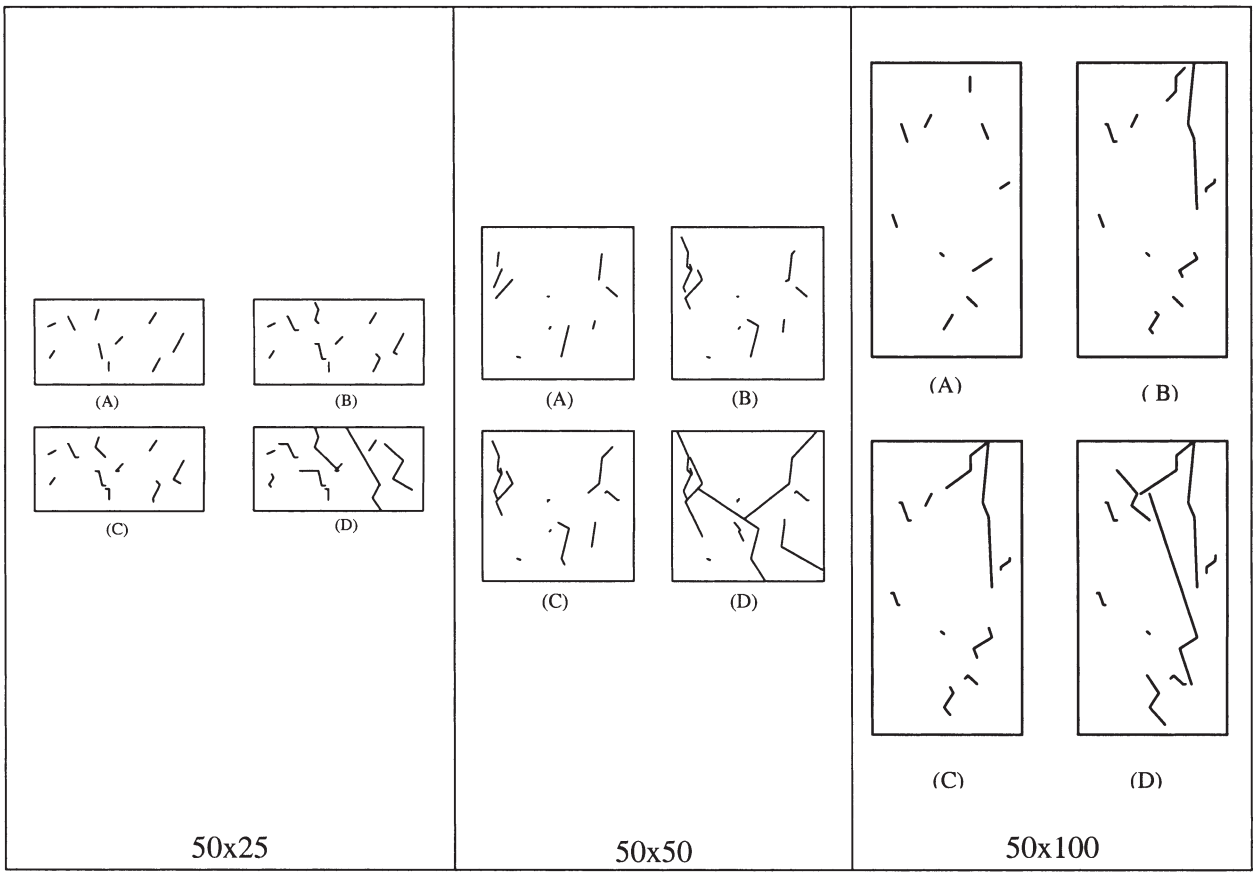

Fig. 5 Numerical crack schemes during a particular simulation (frictionless). (A) represents the initial preloaded state; (B), (C) and (D) represent loaded states as identified in Figs 2, 3 and 4.

elasticity. This particular aspect plays a fundamental role in the real behaviour of the material.

The role of the two different compliances is clear: C' for diffusing microcracks, C'' for local meso- and macro-cracks. This separation of role is also necessary to reduce the time for computational solutions.

Here, as in previous work,[18–20] the hypothesis is made that the decay of the elastic modulus depends on the energy absorbed in the material: the larger the energy absorbed, the lower the elastic modulus. Assuming for the material-matrix a simple linear softening branch, this behaviour is approximated satisfactorily by a decreasing function of the form:[13,14]

$$E^* = E\left(\frac{a}{\sqrt{W}} + b\right) \tag{5}$$

where E is the initial elastic modulus, E^* is the decayed post-peak elastic modulus and W is the strain energy density absorbed during the loading process. The two constants a and b are obtained respecting the two conditions: the initial value (at the peak) of E^* is the real elastic modulus E and its final value is zero. The initial and final values of W and the elastic modulus E are obtained from average values of the experimental curves.

EXPERIMENTAL AND NUMERICAL RESULTS

In this section, a comparison between the experimental results and the numerical simulations will be presented. The comparison concerns the prismatic specimens with a square base (50 mm × 50 mm, 100 mm × 100 mm, 150 mm × 150 mm) and with three different slendernesses (0.5, 1.0, 2.0), with and without friction between the specimen and the loading platens, for a total of 18 cases.

The friction condition is represented by the direct contact between specimen and platens, as the shearing stresses at the interface arise in opposition to the lateral expansion of the specimen. From the computational point of view, this phenomenon is modelled by dividing the loaded boundaries into two parts and by imposing on each part a shearing stress directed inwards.

On the other hand, the introduction of teflon layers between the specimen and the loading platens allows for the lateral expansion of the material. As a consequence,

the shearing stresses at the interface become negligible (the friction coefficient is close to 0.01). In the related numerical simulations, at the boundary there is only the compressive normal stress.

The experimental and numerical results are presented in Figs 2–4, whereas Fig. 5 shows an example of crack evolution during the numerical simulation. For each experimental result three numerical simulations, with different initial crack distribution, have been performed.

The initial meso- and macro-crack density in the analyses is based on the self-similarity random distribution proposed by Carpinteri.[21] Some numerical

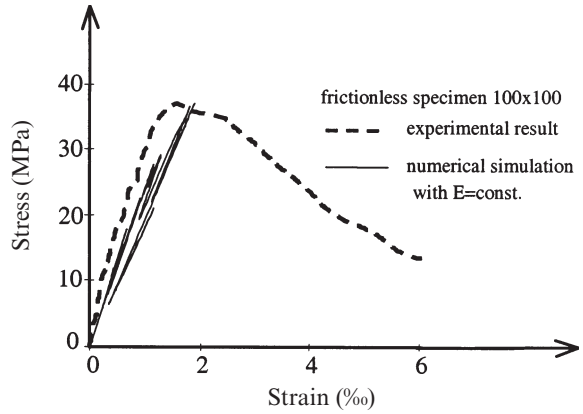

Fig. 6 Stress–strain diagram, the elastic modulus being constant, during the loading simulation.

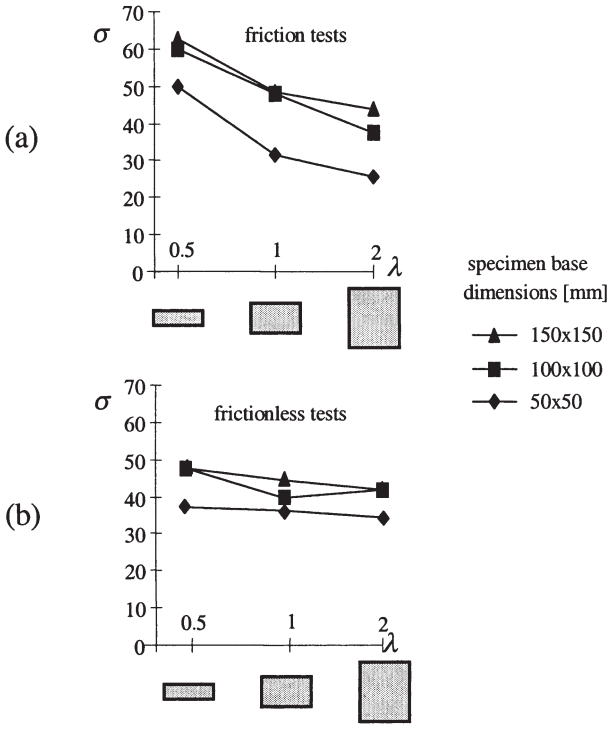

Fig. 7 Variation in strength σ (MPa) by varying the slenderness λ.

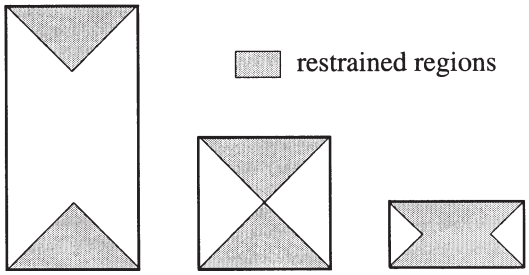

Fig. 8 Restrained regions in friction specimens.

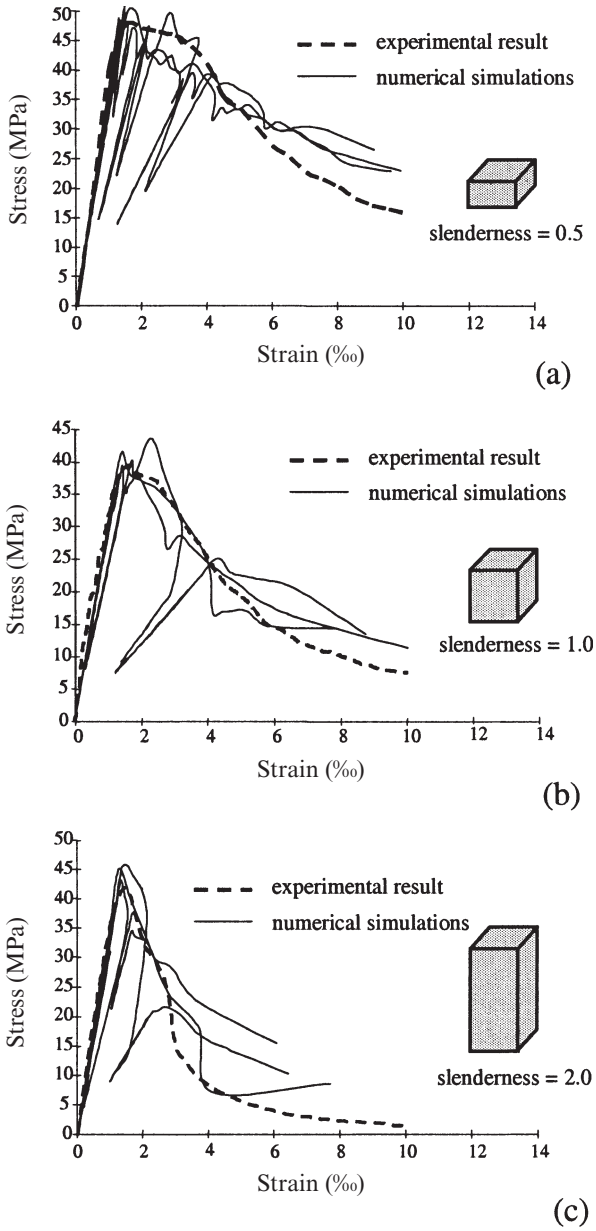

Fig. 9 Variation in the softening branch by varying the specimen slenderness (side length of specimen base: 100 mm).

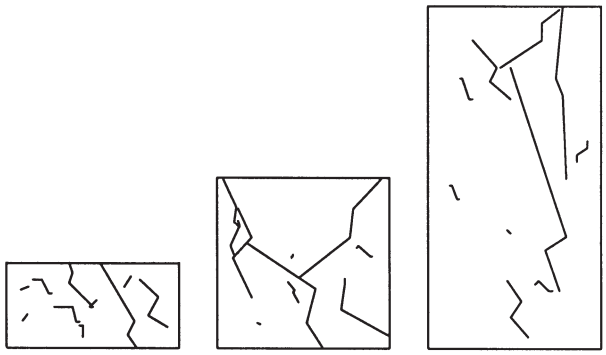

Fig. 10 Different numerical (meso- and macro-cracked) collapse schemes by varying the specimen slenderness.

examples of initial meso- and macro-crack distribution are shown in Fig. 5 (points A).

Snap-back instabilities (see Carpinteri[22]) are observed in the crack-propagation-controlled numerical simulations, the crack length being always growing. However, they were not captured by the displacement controlled experimental tests, the displacement decreasing in the snap-back branches.

DISCUSSION AND CONCLUSIONS

The analysis of the results presented in the paper shows a satisfactory correspondence between the numerical simulations and the experimental tests. A consequence of performing a two-dimensional analysis of a three-dimensional problem is that the cases related to small and stubby specimens with friction (triaxial compression) present some unavoidable differences. These differences are due to the fact that, in these conditions, the real specimen behaviour moves away from the idealized two-dimensional case. The numerical model, however, gives good results in the remaining cases, confirming the validity of the theoretical assumptions on which it is based.

In this regard, it is important to emphasize the centrality of the cracking phenomenon in the structural response. Although the structural collapse is mainly governed by meso- and macrocracks, at the same time it is very important to take into account the widespread elastic decay due to the presence of microcracks. It allows the capture of the softening branch, which is typical of quasi-brittle materials and otherwise not reproducible (Fig. 6).

If the stress–strain response is considered, some interesting aspects arise, which were also shown in other studies.[23,24] First of all, it is important to highlight the friction influence. For all the geometries the following aspects clearly emerge: in the friction cases there is a considerable variation in strength by varying the slenderness [Fig. 7(a)]; the same trend is very mitigated or even absent in frictionless cases [Fig. 7(b)].

As a matter of fact, the frictional shearing stresses acting at the interface produce triaxially confined regions near the bases. For small values of slenderness, the confined regions include most of the specimen (Fig. 8). As a consequence, the maximum loading capacity is higher for stubby specimens (it is well-known that the

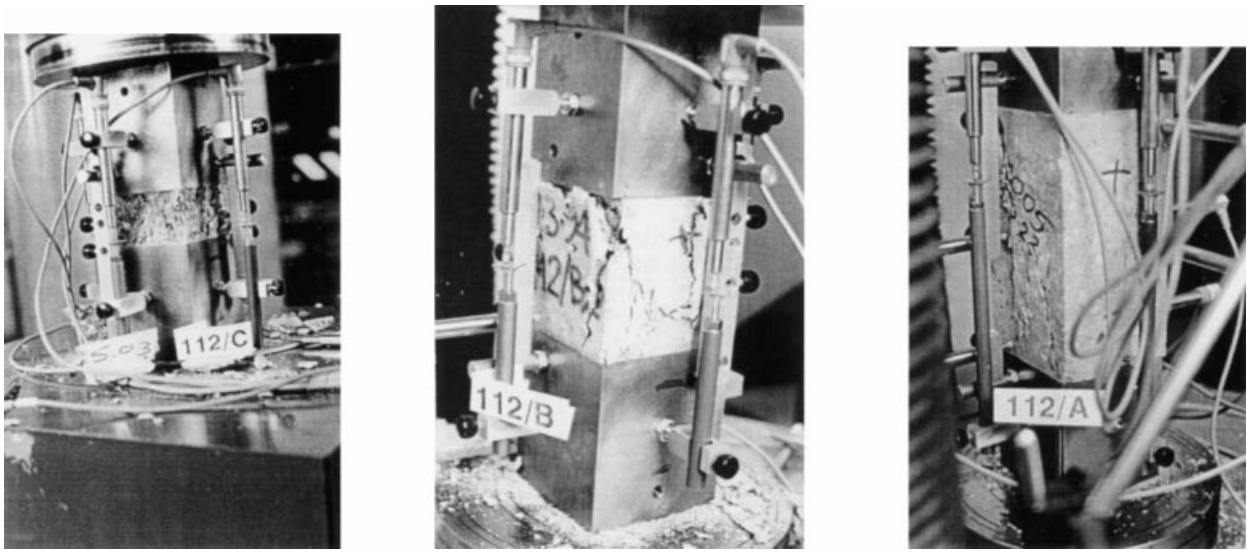

(a) Crushing (b) Intermediate failure (c) Splitting

Fig. 11 Different experimental collapse mechanisms (tests without friction) by increasing the specimen slenderness: crushing, shear cracking and splitting.

triaxial compressive strength is larger than the uniaxial compressive strength). Hence it is possible to explain the variation in strength by varying the slenderness in the friction tests, and the absence of this phenomenon when the teflon layers are used.

An additional important trend is represented by the ductility increase versus the specimen slenderness decrease (Fig. 9). This trend, emerging in all the test results more or less clearly, is connected with and has a justification in the structural collapse schemes. When the slenderness decreases, a transition from splitting to crushing collapse occurs. The numerical simulations confirm the same trend (Fig. 10) of the experimental collapse mechanisms (Fig. 11). However, the crushing collapse is represented by the strong decay of the elastic modulus during the simulations.[13,14] It is characterized by a multitude of microcracks and a larger energy dissipation during rupture and therefore it is associated with a more ductile behaviour. On the contrary, the splitting collapse, which is characterized by a more localized rupture, requires a smaller energy dissipation and then produces a more brittle behaviour.

Acknowledgements

The present research was carried out with the financial support of the Ministry of University and Scientific Research (MURST), the National Research Council (CNR) and the EC-TMR Contract No. ERBFMRXCT960062.

REFERENCES

1 Ferrara, G. and Gobbi, M. E. (1995) *Strain Softening of Concrete under Compression*. Report to RILEM Committee 148 SSC. ENEL-CRIS Laboratory, Milano, Italy.
2 Horii, H. and Nemat-Nasser, S. (1987) Elastic field of interacting inhomogeneities. *Int. J. Solids Structures.* **21,** 731–745.
3 Kachanov, M. and Montagut, E. (1986) Interaction of crack with certain microcrack arrays. *Engng Fract. Mech.* **25,** 625–636.
4 Kachanov, M. (1987) Elastic solids with many cracks and related problems. *Advances Appl. Mech.* **30,** 259–445.
5 Crouch, S. L. and Starfield, A. M. (1983). *Boundary Element Methods in Solid Mechanics*. George Allen & Unwin, London.
6 Brencich, A. and Carpinteri, A. (1996) Interaction of a main crack with ordered distributions of microcracks: a numerical technique by displacement discontinuity boundary elements. *Int. J. Fract.* **76,** 373–389.
7 Sneddon, N. I. and Lowengrub, M. (1969). *Crack Problems in the Classical Theory of Elasticity.* John Wiley & Sons, Inc., Town.
8 Yang, G. P. and Liu, X. L. (1991) Microcracks interaction in concrete. In: *Proceedings of International Symposium on Concrete Engineering*, Nanjing, China.
9 Carpinteri, A., Scavia, C. and Yang, G. P. (1996) Microcrack propagation, coalescence and size effects in compression. *Engng Fract. Mech.* **54,** 335–347.
10 Carpinteri, A. and Yang, G. P. (1996) Fractal dimension evolution of microcrack net in disordered materials. *Theoret. Appl. Fract. Mech.* **25,** 73–81.
11 Carpinteri, A. and Yang, G. P. (1997a) Damage process in finite sized brittle specimen with interacting microcracks. *Fatigue Fract. Engng Mater. Struct.* **20,** 1105–1115.
12 Carpinteri, A. and Yang, G. P. (1997b) Size effects in brittle specimen with microcrack interaction. *Computers & Struct.* **63,** 429–437.
13 Carpinteri, A., Ciola, F. and Pugno, N. (2001) Boundary element method for the strain-softening response of quasi-brittle materials in compression. *Computers & Struct.* **79,** 389–401.
14 Carpinteri, A., Ciola, F. and Pugno, N. (1998) Numerical methods for the strain-softening response of concrete in uniaxial compression. In: *Damage and Fracture Mechanics*, Bologna, Italy. (Edited by A. Carpinteri and C. Brebbia). Computational Mechanics Publications, Southampton, UK, pp. 297–306.
15 Carpinteri, A., Ciola, F., Pugno, N., Ferrara, G. and Gobbi, M. E. (1998) Application of the Boundary Elements Method to the compressive strain-softening behaviour of concrete. In: *Fracture Mechanics of Concrete Structures*, Gifu, Japan. (Edited by H. Mihashi and K. Rokugo). Aedificatio Publishers, Freiberg, Germany, pp. 1949–1962.
16 Erdogan, F. and Sih, G. C. (1963) On the crack extension in plates under plane loading and transverse shear. *J. Basic Engng.* **85,** 519–527.
17 Carpinteri, A. (1997) *Structural Mechanics: A Unified Approach.* E & FN Spon, London, UK.
18 Sih, G. C. and Madenci, E. (1983) Crack growth resistance characterized by the strain energy density function. *Engng Fract. Mech.* **18,** 1159–1171.
19 Carpinteri, A. and Sih, G. C. (1984) Damage accumulation and crack growth in bilinear materials with softening: application of strain energy density theory. *Theoret Appl. Fract. Mech.* **1,** 145–160.
20 Carpinteri, A. (1986) *Mechanical Damage and Crack Growth in Concrete*. Martinuus Nijhoff Publishers, Dordrecht, The Netherlands.
21 Carpinteri, A. (1989) Decrease of apparent tensile and bending strength with specimen size: two different explanations based on fracture mechanics. *Int. J. Solids Struct.* **25,** 407–429.
22 Carpinteri, A. (1989) Softening and snap-back instability in cohesive solids. *Int. J. Numer. Meth. Engng* **28,** 1521–1537.
23 Van Mier, J. G. M. (1984) Strain softening of concrete under multiaxial compression. Ph.D. Thesis. Eindhoven University of Technology, Eindhoven, The Netherlands.
24 Anon. (1997) Strain softening of concrete in uniaxial compression. Report of the Round Robin Test carried out by RILEM TC, 148, SSC. *Mater. Struct.* **30,** 195–209.